

# Redox Behavior and Transport Properties of Composites Based on $(\text{Fe,Ni})_3\text{O}_{4\pm\delta}$ for Anodes of Solid Oxide Fuel Cells<sup>1</sup>

V. A. Kolotygin<sup>a,\*</sup>, V. A. Noskova<sup>a,b</sup>, S. I. Bredikhin<sup>a</sup>, and V. V. Kharton<sup>a</sup>

<sup>a</sup>*Institute of Solid State Physics, Russian Academy of Sciences, Chernogolovka, Moscow oblast, 142432 Russia*

<sup>b</sup>*National University of Science and Technology MISiS, Moscow, 119991 Russia*

\**e-mail: kolotygin@issp.ac.ru*

Received August 2, 2017; in final form, January 12, 2018

**Abstract**—The Fe–Ni–O system designed for producing bimetal-containing composite anodes of solid oxide fuel cells (SOFCs) was studied. The solubility of nickel in the structure of spinel  $(\text{Fe,Ni})_3\text{O}_{4\pm\delta}$  at atmospheric oxygen pressure is  $\sim 1/3$ . Moderate reduction at 1023 K and  $p(\text{O}_2) \approx 10^{-20}$  atm leads to partial decomposition of spinels, forming an electron-conducting phase  $(\text{Fe,Ni})_{1-y}\text{O}$  and submicron bimetallic Fe–Ni particles on the oxide surface, which have potentially high catalytic activity. The electron conductivity has a thermally activated character and increases substantially during the reduction. In the anode conditions of SOFCs, the electric conductivity reaches 30–100 S/cm, while the thermal expansion coefficients are  $\sim 12 \times 10^{-6} \text{ K}^{-1}$ , which ensures compatibility with solid electrolytes. At the same time, significant volume changes during the redox cycling (up to  $\sim 1\%$  on the linear scale) necessitate the introduction of additional components such as yttria-stabilized zirconia (YSZ). The polarization resistance of the model composite anode of reduced  $\text{Fe}_2\text{NiO}_{4\pm\delta}$  and YSZ deposited on the YSZ solid electrolyte membrane was  $\sim 1.8 \text{ Ohm cm}^2$  at 923 K in a 4%  $\text{H}_2$ –Ar– $\text{H}_2\text{O}$  atmosphere.

**Keywords:** SOFC anode, spinel, cermet, electron conductivity, Seebeck coefficient, thermal expansion, chemical expansion, polarization resistance

**DOI:** 10.1134/S1023193518060071

## INTRODUCTION

The materials mainly used today as anodes of solid oxide fuel cells (SOFCs) are metal–ceramic composites (cermets) that include nickel, which provides the electron conductivity and electrochemical activity of the anode, and an oxide (e.g., zirconia) phase, which allows mechanical stabilization of the electrode layer and expansion of the electrochemical reaction zone due to the ion conductivity [1–3]. The high Ni content ( $> (50\text{--}70) \text{ vol } \%$ ) can lead to degradation because of the agglomeration of metal particles, their oxidation at high anode currents, and catalytic activity in the Boudouard reaction (carbon deposition). Therefore, it is important to search for new anode materials with lower nickel contents. These include cermets, where metal alloys or mixtures such as Fe–Ni, Fe–Co, Ni–Cu, etc. are used as electron conductors [4–10]. For example, for SOFCs with a multilayer anode, where the Fe–Ni alloy was used as a current collector layer, the specific power of 400–600 mW/cm<sup>2</sup> was achieved at 873–923 K. Under the oxidative conditions, NiO

partially interacted with  $\text{FeO}_x$  to form a compound with a structure of spinel  $(\text{Fe,Ni})_3\text{O}_4$  [5]. The bimetal-containing anodes and catalysts based on this system provide significant advantages when used in hydrocarbon atmospheres [5, 11–13].

At the same time, the information on the thermodynamic limits of existence of phases, kinetics of phase transitions in the Fe–Ni–O system, and corresponding changes in the functional properties of materials in the mid-temperature range (750–1050 K), which is critical for the development of SOFCs, is scanty. The phase equilibria, defect formation, and transport mechanisms in this system were systematically studied for temperatures above 1270–1370 K (for example, [14–16]). While the basic electronic transport mechanisms persist in a wide range of temperatures, the behavior of oxide and composite materials under conditions close to those of SOFC functioning is characterized by the significantly increasing role of the morphology, surface processes, and stability of thermodynamically metastable states [14–19].

The present study is devoted to the synthesis and investigation of the spinels  $\text{Fe}_{3-x}\text{Ni}_x\text{O}_{4\pm\delta}$  ( $0.4 \leq x \leq 1.5$ ) and composites based on them for use as precursors of

<sup>1</sup> Presented at the IV All-Russian Conference “Fuel Cells and Fuel Cell based Power Plants” (with international participation) June 25–29, 2017, Suzdal, Vladimir region.

bimetal-containing anodes and catalysts. The study focused on the analysis of phase stability, thermal expansion, electric conductivity, and thermomechanical behavior of the materials during the oxygen chemical potential cycling. The electrochemical activity of the model composite electrodes obtained by partial reduction of  $(\text{Fe,Ni})_3\text{O}_{4\pm\delta}$  were evaluated.

## EXPERIMENTAL

The materials of the composition  $\text{Fe}_{3-x}\text{Ni}_x\text{O}_{4\pm\delta}$  ( $0.4 \leq x \leq 1.5$ ) were synthesized by the glycine-nitrate method, which allows homogeneity and high dispersity of the oxide products of the reaction. Nickel nitrate and iron oxalate were used as the starting reagents. The exact water content in crystalline hydrates was determined by thermogravimetry using a Setaram Setsys Evolution 16/18 analyzer (France). The nickel and glycine nitrate samples were dissolved in water, where a solution of an iron salt in nitric acid was subsequently added. The glycine sample was calculated in 1.5-fold excess relative to the total content of nitrate groups in  $\text{Ni}(\text{NO}_3)_2$  and  $\text{HNO}_3$  consumed on dissolution of iron oxalate. At the next stages, water was evaporated until self-ignition, after which the resulting foam mixture was dried at 473 K and calcinated at 1073 K to remove water, unchanged nitrates, and organic components.

To prepare dense ceramic samples, we used uniaxial hydraulic press molding of powders into disks with a diameter of 10–20 mm and a thickness of 0.6–1.5 mm at a pressure of 50–100 MPa. A similar molding process was used to prepare  $\text{Zr}_{0.85}\text{Y}_{0.15}\text{O}_{2-\delta}$  (8YSZ) solid electrolyte membranes from HSY-8 commercial powder (Daiichi Kigenso Kagaku Kogyo, Japan). The molded disks were sintered in air or required gas atmosphere in the temperature range 1473–1673 K. For conductivity, Seebeck coefficient, and dilatometry measurements, the samples in the form of bars were cut out of the resulting ceramic disks using a TechCut 4 precision cutting machine (Allied, United States).

The  $\text{Fe}_2\text{NiO}_{4\pm\delta}$ –8YSZ composite powders were obtained by mixing the powder of the synthesized oxide phase with the 8YSZ powder in an appropriate ratio and then grinding the mixture in a Pulverisette 5 planetary ball mill (Fritsch, Germany) with zirconia balls.

To study the stability of the materials under reductive conditions, the powders were annealed in a 4%  $\text{H}_2$ –Ar– $\text{H}_2\text{O}$  mixture. The partial oxygen pressure in the reactor was monitored with a zirconia-based oxygen sensor.

The phase composition of the materials was studied by X-ray phase analysis (XRD). The XRD patterns were obtained with a D-500-Braun X02-1787 diffractometer (Siemens, Germany;  $\text{CuK}_\alpha$  radiation). The unit cell parameters of the single-phase composites were calculated with PowderCell software. The pow-

ders, ceramics, and electrode layers were studied by electron microscopy before and after electrochemical measurements using a Supra 50VP high-resolution scanning electron microscope (LEO Carl Zeiss, Germany). The dilatometric studies were performed using an L75/N1 vertical dilatometer (Linseis, Germany). To evaluate the thermal expansion, the measurements were performed in an air or argon flow depending on the material in a continuous heating mode of up to 1373 K and at a cooling rate of 3 K/min. The isothermal measurements of chemical expansion were performed at 973 K in a mode of atmosphere switchover in a sequence “air → Ar → 4%  $\text{H}_2$ –Ar → Ar → air → Ar → 4%  $\text{H}_2$ –Ar → Ar → air” at storage times of 0.5–3.0 h. The partial oxygen pressure in the gas mixture that exits from the dilatometer was determined using an electrochemical sensor. The specific electric conductivity was measured by a DC four-probe method. The conductivity and Seebeck coefficient were measured in an air or argon flow and in a unit with electrochemical control of the gas medium composition [20].

To prepare a paste for electrode layer deposition, a Heraeus V-006A binder (Germany) was added to the composite powder in a 1 : 1 mass ratio, and the mixture was stirred in an ARE-250 planetary mixer (Thinky, Japan). The paste was deposited on both sides of the solid electrolyte membrane by printing; then it was annealed at 1473 K in air for 2 h. The surface density of the electrodes after annealing was 5–10  $\text{mg}/\text{cm}^2$ .

The polarization resistance was measured by impedance spectroscopy in a cell with symmetric anodes using an Autolab 302 NPGSTAT potentiostat galvanostat (The Netherlands) with a built-in FRA-32M2 module in the frequency range 1 mHz–2 MHz.

## RESULTS AND DISCUSSION

According to the XRD data (Fig. 1), the solubility of nickel in the lattice of  $\text{Fe}_{3-x}\text{Ni}_x\text{O}_{4\pm\delta}$  lies in the range 33–50 at %. The excess amount of nickel ( $x = 1.5$ ) leads to the formation of an NiO-based impurity (Fig. 1d), while the absence of impurities on the XRD pattern of  $\text{Fe}_2\text{NiO}_{4\pm\delta}$  after the synthesis in air or oxygen was achieved only with slow cooling (Fig. 1a). This behavior is consistent with the phase diagram of  $\text{Fe}_2\text{O}_3$ –NiO at atmospheric oxygen pressure (Fig. 2), according to which the  $(\text{Fe,Ni})_3\text{O}_{4\pm\delta}$  solid solutions with a spinel structure are formed in air up to ~33 at % and at temperatures below 1473 K. The microscopic analysis of  $\text{Fe}_2\text{NiO}_{4\pm\delta}$  ceramics (Fig. 3a) revealed domains (10–50  $\mu\text{m}$ ) enriched with nickel and separated from the main phase by a distinct boundary. According to the phase diagram and microprobe X-ray fluorescence analysis data (Table 1), the product of partial decomposition of spinel is the bunsenite phase  $(\text{Ni,Fe})_{1-y}\text{O}$ , which explains the increased nickel content in the domains. From the viewpoint of formation of

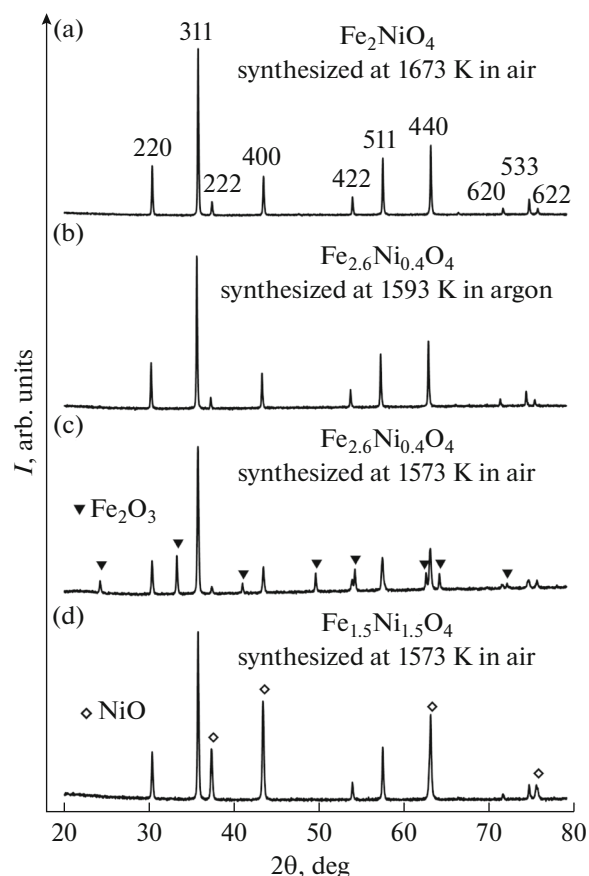


**Fig. 1.** X-ray diffraction patterns of  $\text{Fe}_{3-x}\text{Ni}_x\text{O}_{4\pm\delta}$  powders at  $x =$  (a) 1, (b, c) 0.4, and (d) 1.5 after the synthesis in (a, c, d) air and (b) argon.

electrode materials, these domains can favor the formation of highly disperse metal particles—catalytic centers under the reduction conditions.

**Table 1.** Results of microprobe element analysis obtained in zones 1, 2, and 3 in Fig. 3a

Zone	Fe : Ni ratio (at.)
1	1 : 7.7
2	1 : 3.5
3	2.1 : 1

**Table 2.** Unit cell parameters, activation energy of specific electric conductivity, and average thermal expansion coefficients of  $\text{Fe}_{3-x}\text{Ni}_x\text{O}_{4\pm\delta}$

Material	Atmosphere in the synthesis and measurements	$a$ , nm	Electric conductivity		Thermal expansion	
			$T$ , K	$E_a$ , kJ/mol	$T$ , K	$\text{TEC} \times 10^6$ , $\text{K}^{-1}$
$\text{Fe}_2\text{NiO}_{4\pm\delta}$	Air $p(\text{O}_2) = 0.21$ atm	0.8337(2)	650–900	$110 \pm 4$	900–1370	$11.9 \pm 0.1$
$\text{Fe}_{2.6}\text{Ni}_{0.4}\text{O}_{4\pm\delta}$	Argon $p(\text{O}_2) = 10^{-6} - 10^{-4}$ atm	0.8362(2)	800–1010	$63 \pm 9$	900–1370	$11.8 \pm 0.1$

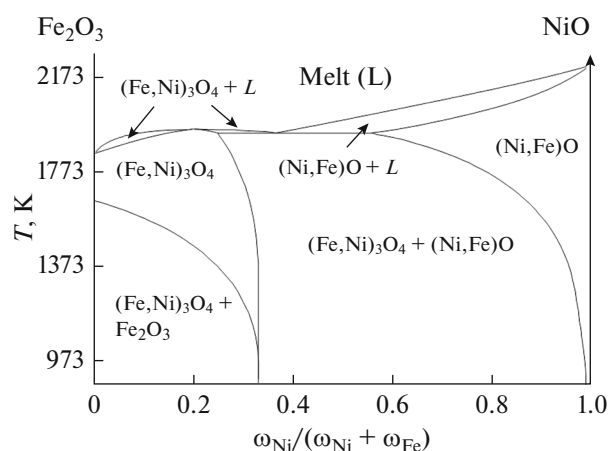


**Fig. 2.** Phase diagram of  $\text{Fe}_2\text{O}_3$ – $\text{NiO}$  in air constructed based on the data of [28, 29].

The single-phase powders and  $\text{Fe}_{2.6}\text{Ni}_{0.4}\text{O}_{4\pm\delta}$  ceramics were obtained only in inert atmospheres (for example, in argon at  $p(\text{O}_2) \approx 10^{-5}$  atm), while during the synthesis in air or subsequent oxidation, the hematite  $\text{Fe}_2\text{O}_3$  phase formed (Figs. 1b and 1c), which has low electric conductivity. Therefore, the transport and thermomechanical properties of this material were studied in an argon atmosphere.

The observed solubility limit of nickel in  $(\text{Fe,Ni})_3\text{O}_{4\pm\delta}$  is very close to the fraction of tetrahedral sites in the spinel lattice, which, at first sight, suggests the formation of a direct spinel structure in which all octahedral sites are occupied by  $\text{Fe}^{3+}$  cations, and the  $\text{Ni}^{2+}$  ions lie in the tetrahedral sublattice (1/3 of the total number of cationic sites). This assumption, however, contradicts the literature data, which showed high tendency for nickel to occupy the octahedral sites [21–23]. The degree of inversion ( $\gamma$ ) corresponding to the dopant fraction in the octahedral sublattice of  $[\text{Fe}_{2-\gamma}\text{Ni}_\gamma]_{\text{oct}}[\text{Fe}_\gamma\text{Ni}_{1-\gamma}]_{\text{tet}}\text{O}_4$  was determined to be  $0.70 \pm 0.28$  [22]. The lattice parameters of spinel (space group  $Fm\bar{3}m$ ) decrease when the nickel concentration increases (Table 2). If the cation nonstoichiometry is assumed to be insignificant, this tendency may be explained by the partial replacement of low-spin  $\text{Fe}^{2+}$  cations ( $r_{\text{ion}} = 0.063$  nm) by  $\text{Ni}^{2+}$  cations

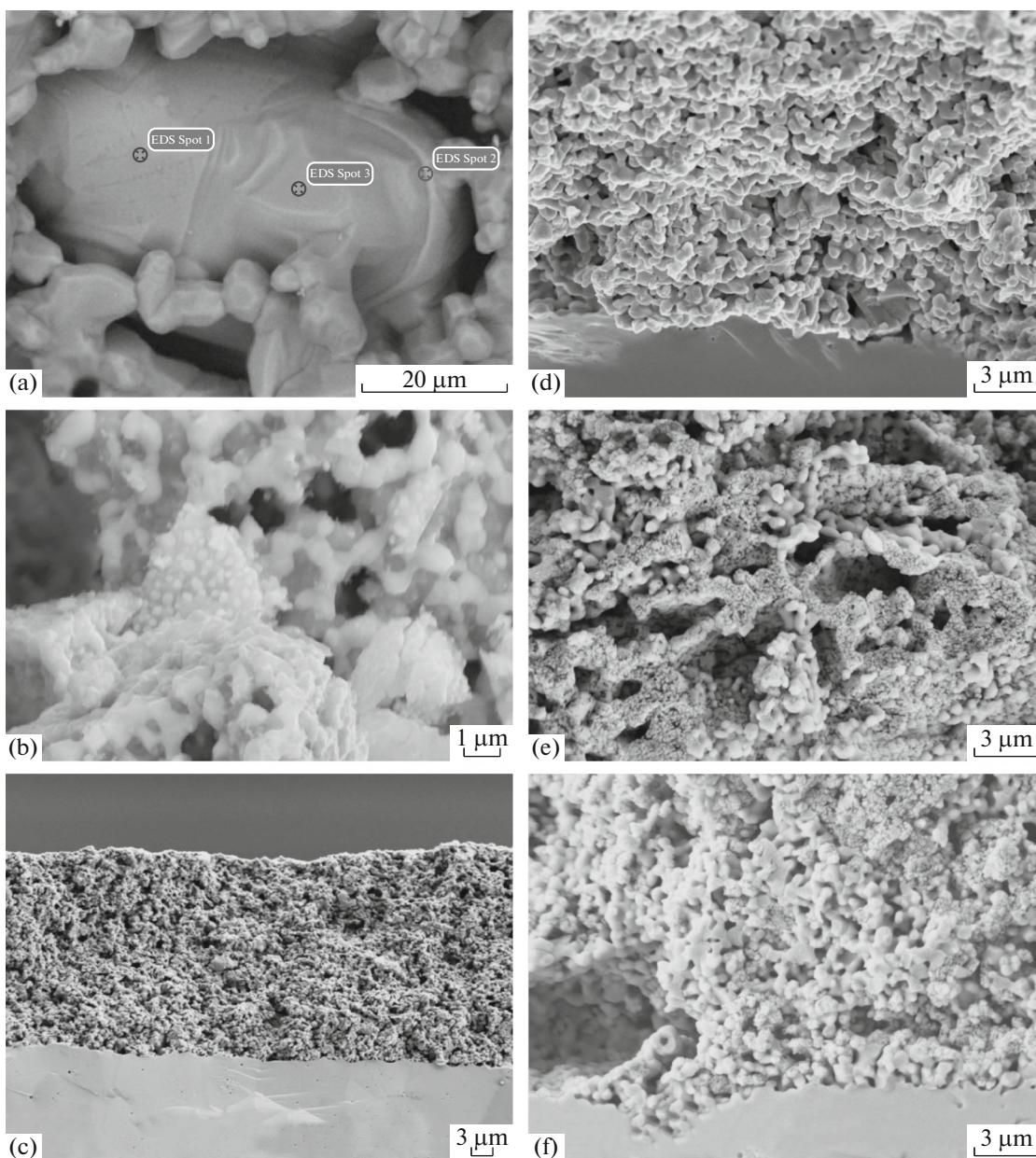


**Fig. 3.** Micrographs of the (a)  $\text{Fe}_2\text{NiO}_{4\pm\delta}$  ceramics after annealing at 1673 K in air, (b)  $\text{Fe}_2\text{NiO}_{4\pm\delta}$  powder after annealing at 973 K in 4%  $\text{H}_2\text{-Ar-H}_2\text{O}$ , and (c)  $\text{Fe}_2\text{NiO}_{4\pm\delta}\text{-8YSZ}$  (80–20 vol %) electrode layer deposited on the 8YSZ membrane and burnt-in at 1473 K in air; (d–f)  $\text{Fe}_2\text{NiO}_{4\pm\delta}\text{-8YSZ}$  (50–50 vol %) electrode layer reduced at (d) 873 K for 1 h, (e) 923 K for 5 h, and (f) 973 K for 25 h.

( $r_{\text{ion}} = 0.055$  nm) mainly in the tetrahedral sublattice because in the case of analogous replacement at the octahedral sites, the lattice parameter would change oppositely, while the difference between the cation radii of  $\text{Fe}^{3+}$  and  $\text{Ni}^{3+}$  is insignificant [24].

The reduction of the materials under anodic conditions leads to the formation of  $(\text{Fe},\text{Ni})_{1-y}\text{O}$  solid solutions and the  $\text{Fe}_3\text{Ni}$  metal phase (Fig. 4). In a moistened 4%  $\text{H}_2\text{-Ar}$  mixture at  $p(\text{O}_2) \approx 3.5 \times 10^{-20}$  atm and

1023 K, the bimetallic fraction is 10–30% (Table 3). An increase in the nickel content reduces the proportion of oxides in accordance with the greater tendency for nickel to be reduced compared to that of iron [16]. The electron microscopic analysis showed the presence of metal particles with a diameter of 100–500 nm on the surface of the oxide phase (Fig. 3b).

The dilatometric curves of  $\text{Fe}_{3-x}\text{Ni}_x\text{O}_{4\pm\delta}$  show a gradual increase in the thermal expansion coefficients

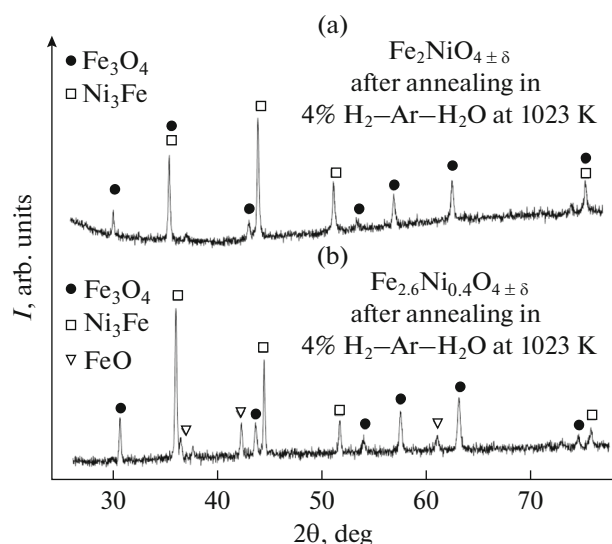


**Fig. 4.** X-ray diffraction patterns of  $\text{Fe}_{3-x}\text{Ni}_x\text{O}_{4\pm\delta}$  at (a)  $x = 1$  and (b)  $0.4$  after annealing at  $973\text{ K}$  in  $4\% \text{ H}_2\text{-Ar-H}_2\text{O}$ .

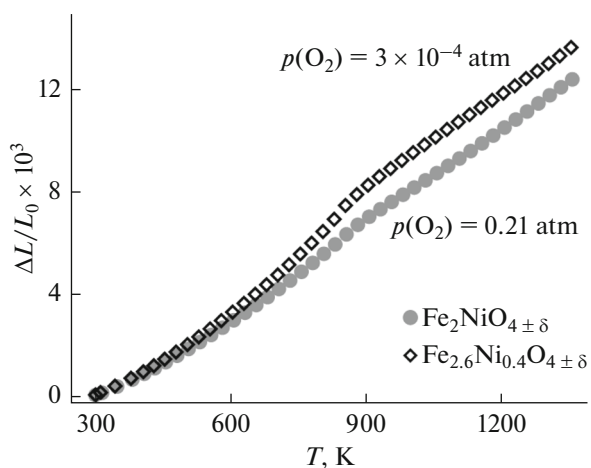


**Fig. 5.** Temperature dependences of relative elongation obtained in the permanent heating mode of the  $\text{Fe}_{3-x}\text{Ni}_x\text{O}_{4\pm\delta}$  ceramics ( $x = 1$  and  $0.4$ ) in air and argon, respectively.

(TECs) on heating to  $\sim 800\text{ K}$ , after which the dependence becomes almost linear (Fig. 5). A similar behavior is characteristic for undoped  $\text{Fe}_3\text{O}_{4\pm\delta}$  [25], in which the ferrimagnet  $\rightarrow$  paramagnet transition occurs at  $600\text{--}800\text{ K}$  [23]. Doping with nickel partially suppresses this transition, and the change in TEC becomes less pronounced. The TECs of materials with  $x = 1$  and  $0.4$  in the high-temperature range is  $\sim 12 \times 10^{-6}\text{ K}^{-1}$  in air and argon, respectively (Table 2). This level of expansion is acceptable for the production of electrode layers. However, the chemical expansion caused by changes in the composition of the oxide phase and/or phase transformations during the reduc-

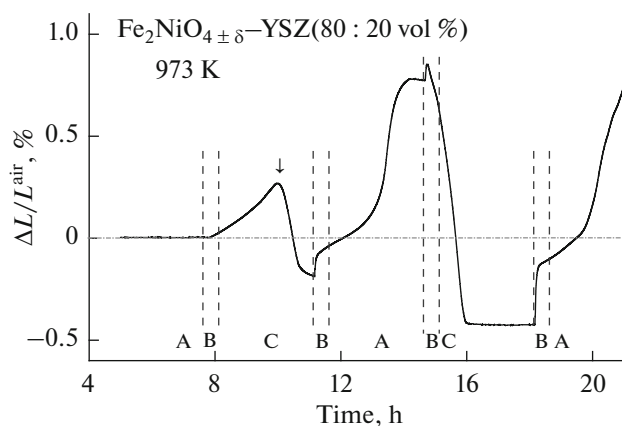


**Fig. 6.** Isothermal dependence of relative elongation on time for the  $\text{Fe}_2\text{NiO}_{4\pm\delta}\text{-YSZ}$  ( $80\text{:}20\text{ vol } \%$ ), ceramics obtained in the cycling mode of the chemical potential of oxygen. The zones marked at the bottom of the figure correspond to the gases: A—air, B—argon, and C— $4\% \text{ H}_2\text{-Ar-H}_2\text{O}$  mixture. The vertical arrow marks the maximum elongation during the initial reduction (see text).

tion represents a problem. In particular, in the isothermal redox cycling of the  $\text{Fe}_2\text{NiO}_{4\pm\delta}\text{-YSZ}$  composite ( $80\text{--}20\text{ vol } \%$ ) in the sequence shown in Fig. 6, the linear dimensional changes are up to  $1\%$ . At the initial stage of the reduction of the material (up to the point indicated by the vertical arrow in Fig. 6), the expansion is  $\sim 0.25\%$  due to the increased  $\text{Fe}^{2+}$  concentration and the isolation of the  $(\text{Fe,Ni})_{1-y}\text{O}$  phase. Further reduction leads to the formation of a metal phase with higher density and hence to  $\sim 0.5\%$  compression. The amplitude of chemical expansion increases during subsequent redox cycling as a result of the microstructural changes associated with phase segregation and acceleration of transition kinetics. Although the observed volume increments are significantly lower than the analogous parameters for the reduction of NiO [26, 27], the YSZ content should be increased to ensure the thermomechanical stability of anodes for further reduction of chemical expansion.

The electric conductivity of  $\text{Fe}_{3-x}\text{Ni}_x\text{O}_{4\pm\delta}$  spinels exhibits a thermally-activated character (Fig. 7). An increase in the nickel content reduces the conductivity and increases the corresponding activation energy

**Table 3.** Phase composition of  $\text{Fe}_{3-x}\text{Ni}_x\text{O}_{4\pm\delta}$  after 24-h annealing in  $4\% \text{ H}_2\text{-Ar-H}_2\text{O}$  at  $1023\text{ K}$

Starting phase	Phase composition after annealing
$\text{Fe}_{2.6}\text{Ni}_{0.4}\text{O}_{4\pm\delta}$	76% $\text{Fe}_3\text{O}_4$ 12% $\text{Ni}_3\text{Fe}$ 12% $\text{FeO}$
$\text{Fe}_2\text{NiO}_{4\pm\delta}$	69% $\text{Fe}_3\text{O}_4$ 31% $\text{Ni}_3\text{Fe}$

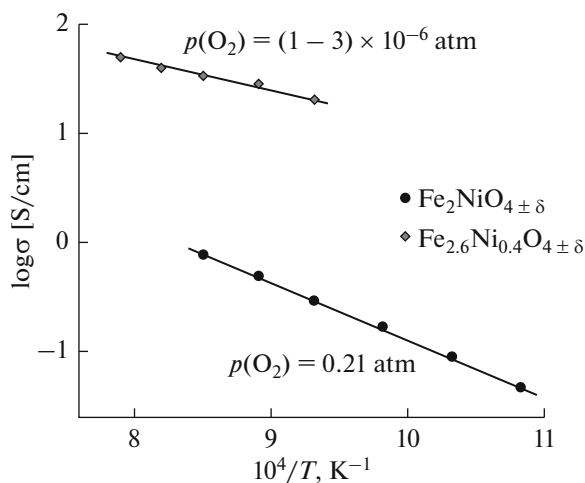


**Fig. 7.** Temperature dependences of the specific electric conductivity of the  $\text{Fe}_{3-x}\text{Ni}_x\text{O}_{4\pm\delta}$  ceramics ( $x = 1$  and  $0.4$ ) in air and argon, respectively.

(Table 2). This behavior suggests the dominant contribution of the  $\text{Fe}^{2+/3+}$  redox pair, while the  $\text{Ni}^{2+}$  cations are largely excluded from the electron transfer. A reduction of the partial oxygen pressure to  $10^{-4}$  atm leads to a moderate increase in conductivity (Fig. 8a). In combination with the negative Seebeck coefficient (Fig. 8b), this clearly suggests the predominant role of  $n$ -type electron charge carriers. The reduction in the intermediate range of oxygen pressures ( $10^{-12}$ – $10^{-6}$  atm at 1173 K for  $\text{Fe}_2\text{NiO}_{4\pm\delta}$ ) does not affect the electric properties, which may be related to the achieved stoichiometric oxygen content ( $\delta \rightarrow 0$ ). This assumption is consistent with the superstoichiometric oxygen content under the oxidation conditions, which can be achieved by formation of cation vacancies [14, 15, 25]. Note that the width of the plateau on the conductivity and thermo-EMF dependences on the partial oxygen pressure (Fig. 8) can increase due to the kinetic factors such as inhibition of the  $(\text{Fe},\text{Ni})_3\text{O}_4 \leftrightarrow (\text{Fe},\text{Ni})_{1-y}\text{O}$  phase transition and low rate of equilibration at intermediate  $p(\text{O}_2)$ , when the concentrations of molecular oxygen and reducing components in the gas phase are extremely low. Further reduction leads to an abrupt increase in electric conductivity, which is more pronounced at elevated temperatures. Based on the data of XRD and microscopic analysis (Figs. 3 and 4), this is due to the formation of the highly conductive  $(\text{Fe},\text{Ni})_{1-y}\text{O}$  and then metallic phases. The specific electric conductivity reaches 30–100 S/cm under anodic conditions at 1173 K.

Because of great changes in the volume during redox cycling (Fig. 6) and high degree of sintering, the deposition of electrode layers based on  $\text{Fe}_2\text{NiO}_{4\pm\delta}$  without additives leads to peeling of the anode from the solid electrolyte membrane. Therefore, model composite electrodes based on  $\text{Fe}_2\text{NiO}_{4\pm\delta}$ –8YSZ

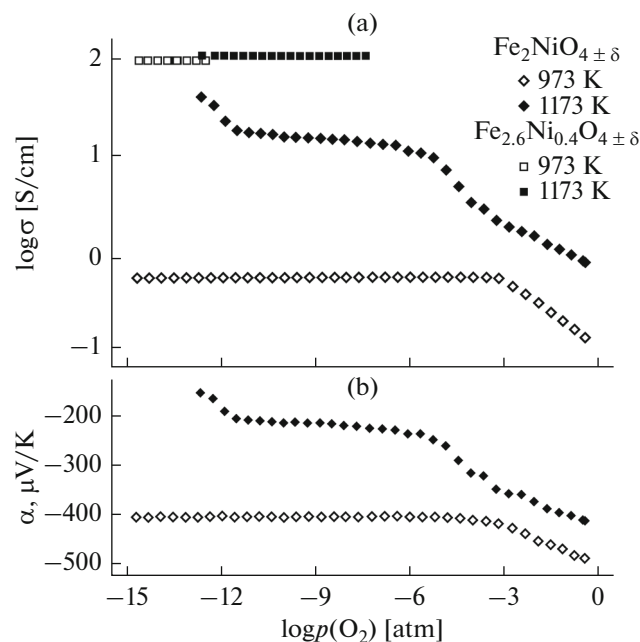


**Fig. 8.** Isothermal dependences of the (a) specific conductivity and (b) Seebeck coefficient of  $\text{Fe}_{3-x}\text{Ni}_x\text{O}_{4\pm\delta}$  on the partial pressure of oxygen.

with 20–70 vol % electron conductor were prepared in order to study the electrochemical behavior. The microstructure of the anode layer with 20 vol % 8YSZ right after the deposition and burning-in is illustrated in Fig. 3c. The anode with a thickness of  $\sim 20$   $\mu\text{m}$  is characterized by sufficiently high porosity, homogeneity, and good adhesion to the solid electrolyte.

Figure 9 presents the examples of the impedance spectra of composite anodes with different 8YSZ contents. The optimum content of the  $\text{Fe}_2\text{NiO}_{4\pm\delta}$  phase in the precursor is 40–60 vol %. For the anode obtained during the reduction of the  $\text{Fe}_2\text{NiO}_{4\pm\delta}$ –8YSZ composite (50–50 vol %), the polarization resistance is 1.8  $\Omega\text{cm}^2$  at 923 K in a humidified 4%  $\text{H}_2$ –Ar gas mixture. Although this value is higher than required for practical use, in the atmospheres of pure hydrogen or partially oxidized hydrocarbon fuels, the electrochemical activity is expected to be much higher. In particular, the impedance hodographs (Fig. 9) show an appreciable low-frequency contribution, which can be due to the hindered mass transfer and slow adsorption. In addition, in order to achieve improved electrochemical characteristics, it is necessary to optimize the microstructure, thickness, and anode reduction conditions. The electron microscopic analysis revealed that the anode reduction at temperatures above 900 K leads to microstructural degradation as a result of additional sintering of the components and the formation of cavities that negatively affect the contact area and the integral electrochemical properties of the electrode layers (Figs. 3d–3f).

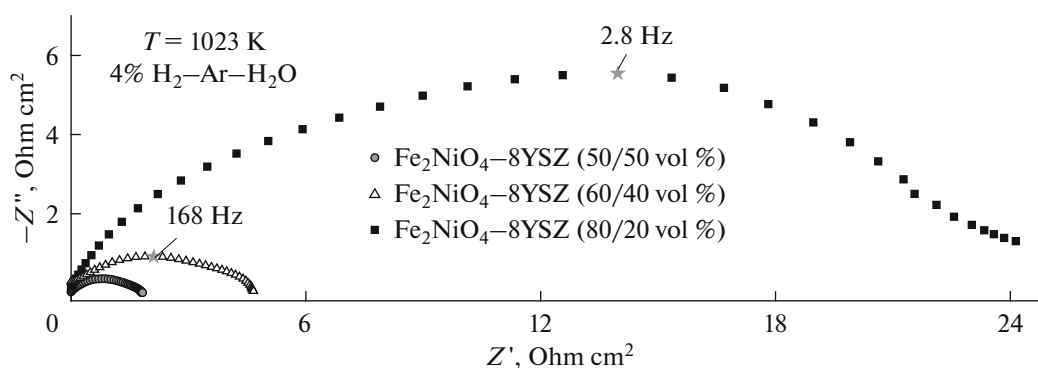


Fig. 9. Impedance hodographs obtained for symmetric composite anodes from reduced  $\text{Fe}_2\text{NiO}_{4 \pm \delta}$  and 8YSZ containing 20, 40, and 50 vol % stabilized zirconia at 923 K in an atmosphere of 4%  $\text{H}_2\text{-Ar-H}_2\text{O}$ .

## CONCLUSIONS

The results of synthesis and studies of the properties of spinels of the  $\text{Fe}_{3-x}\text{Ni}_x\text{O}_{4 \pm \delta}$  system ( $0.4 \leq x \leq 1.5$ ) as precursors of bimetal-containing composite anodes of SOFCs were presented. The solubility of nickel in the magnetite structure at atmospheric oxygen pressure was found to be  $\sim 1/3$  with respect to the total amount of cations, while the decrease in the nickel content reduces the stability of the phase under the oxidation conditions. The reduction at 1023 K in an atmosphere of humidified 4%  $\text{H}_2\text{-Ar}$  gas mixture leads to a segregation of  $(\text{Fe,Ni})_{1-y}\text{O}$  and submicron bimetal particles on the surface of the oxide matrix. The electron conductivity of spinels is due to the migration of  $n$ -type charge carriers and increases with decreasing nickel content. The electric conductivity reaches 30–100 S/cm due to the partial decomposition of spinel with formation of highly conductive phases under anodic conditions. The TEC of ceramic materials is  $\sim 12 \times 10^{-6} \text{ K}^{-1}$ , which provides thermomechanical compatibility with solid electrolytes based on zirconia. The level of volume changes during redox cycling is significantly lower compared to the reduction of NiO, but it does not allow the use of reduced spinels for anode formation without introducing additional oxide components. The introduction of significant amounts of ion-conducting components is also required to suppress sintering and increase the electrochemical activity of the anode layers.

## ACKNOWLEDGMENTS

This study was financially supported by the Russian Scientific Foundation (project no. 17-79-30071). The experimental procedures and measurement benches used in the studies were developed with support from the Ministry of Education and Science of the Russian Federation (Agreement no. 14.B25.31.0018).

## REFERENCES

1. Minh, N.Q., Ceramic Fuel Cells, *J. Am. Ceram. Soc.*, 1993, vol. 76, p. 563.
2. Jiang, S.P. and Chan, S.H., A review of anode materials development in solid oxide fuel cells, *J. Mater. Sci.*, 2004, vol. 39, p. 4405.
3. Tsipis, E.V. and Kharton, V.V., Electrode materials and reaction mechanisms in solid oxide fuel cells: A brief review. II. Electrochemical behavior vs. materials science aspects, *J. Solid State Electrochem.*, 2008, vol. 12, p. 1367.
4. Tsipis, E.V. and Kharton, V.V., Electrode materials and reaction mechanisms in solid oxide fuel cells: A brief review. III. Recent trends and selected methodological aspects, *J. Solid State Electrochem.*, 2011, vol. 15, p. 1007.
5. Park, H.C. and Virkar, A.V., Bimetallic (Ni-Fe) anode-supported solid oxide fuel cells with gadolinia-doped ceria electrolyte, *J. Power Sources*, 2009, vol. 186, p. 133.
6. Lee, S.I., Vohs, J.M., and Gorte, R.J., A study of SOFC anodes based on Cu-Ni and Cu-Co bimetals in  $\text{CeO}_2\text{-YSZ}$ , *J. Electrochem. Soc.*, 2004, vol. 151, p. 1319.
7. Gross, M.D., Vohs, J.M., and Gorte, R.J., Recent progress in SOFC anodes for direct utilization of hydrocarbons, *J. Mater. Chem.*, 2007, vol. 17, p. 3071.
8. Lu, Z.G., Zhu, J.H., Bi, Z.H., and Lu, X.C., A Co-Fe alloy as alternative anode for solid oxide fuel cell, *J. Power Sources*, 2008, vol. 180, p. 172.
9. Konar, R., Mukhopadhyay, J., Sharma, A.D., and Basu, R.N., Synthesis of Cu-YSZ and Ni-Cu-YSZ cermet by a novel electroless technique for use as solid oxide fuel cell anode: Application potentiality towards fuel flexibility in biogas atmosphere, *Int. J. Hydrogen Energy*, 2016, vol. 41, p. 1151.
10. Kim, S., Kim, C., Lee, J.H., Shin, J.B., Lim, T.-H., and Kim, G., Tailoring Ni-based catalyst by alloying with transition metals ( $M = \text{Ni, Co, Cu, and Fe}$ ) for direct hydrocarbon utilization of energy conversion devices, *Electrochim. Acta*, 2017, vol. 225, p. 399.
11. Ringuedé, A., Labrincha, J.A., and Frade, J.R., A combustion synthesis method to obtain alternative cer-

- met materials for SOFC anodes, *Solid State Ionics*, 2001, vol. 141, p. 549.
12. Kan, H. and Lee, H., Enhanced stability of Ni–Fe/GDC solid oxide fuel cell anodes for dry methane fuel, *Catal. Commun.*, 2010, vol. 12, p. 36.
  13. Wang, J.-G., Liu, C.-J., Zhang, Y.-P., Yu, K.-L., Zhu, X.-L., and He, F., Partial oxidation of methane to syngas over glow discharge plasma treated Ni–Fe/Al<sub>2</sub>O<sub>3</sub> catalyst, *Catal. Today*, 2004, vol. 89, p. 183.
  14. Dieckmann, R., Defects and cation diffusion in magnetite (IV): nonstoichiometry and point defect structure of magnetite (Fe<sub>3- $\delta$</sub> O<sub>4</sub>), *Ber. Bunsen-Ges.*, 1982, vol. 86, p. 112.
  15. Kofstad, P., *Otklonenie ot stekhiometrii, diffuziya i elektroprovodnost' v prostykh okislakh metallov* (Nonstoichiometry, Diffusion, and Electric Conductivity in Metal Oxides), Moscow, Mir, 1975.
  16. Tret'yakov, Yu.D., *Khimiya nestekhiometricheskikh oksidov* (Chemistry of Nonstoichiometric Oxides), Moscow: Mosk. Gos. Univ., 1974.
  17. Petric, A. and Ling, H., Electrical conductivity and thermal expansion of spinels at elevated temperatures, *J. Am. Ceram. Soc.*, 2007, vol. 90, p. 1515.
  18. Summerfelt, S.R. and Carter, C.B., Kinetics of NiFe<sub>2</sub>O<sub>4</sub> precipitation in NiO, *J. Am. Ceram. Soc.*, 1992, vol. 75, p. 2244.
  19. Solís, C., Somacescu, S., Palafox, E., Balaguer, M., and Serra, J.M., Particular transport properties of NiFe<sub>2</sub>O<sub>4</sub> thin films at high temperatures, *J. Phys. Chem. C*, 2014, vol. 118, p. 24266.
  20. Patrakeev, M.V., Mitberg, E.B., Lakhtin, A.A., Leonidov, I.A., Kozhevnikov, V.L., Kharton, V.V., Avdeev, M., and Marques, F.M.B., Oxygen nonstoichiometry, conductivity, and Seebeck coefficient of La<sub>0.3</sub>Sr<sub>0.7</sub>Fe<sub>1-x</sub>Ga<sub>x</sub>O<sub>2.65+ $\delta$</sub>  perovskites, *J. Solid State Chem.*, 2002, vol. 167, p. 203.
  21. West, A.R., *Solid State Chemistry and Its Applications*, vol. 2, New York: Wiley, 2014.
  22. Lazarević, Z.Ž., Sekulić, D.L., Ivanovski, V.N., and Romčević, N.Ž., A structural and magnetic investigation of the inversion degree in spinel NiFe<sub>2</sub>O<sub>4</sub>, ZnFe<sub>2</sub>O<sub>4</sub> and Ni<sub>0.5</sub>Zn<sub>0.5</sub>Fe<sub>2</sub>O<sub>4</sub> ferrites prepared by soft mechanochemical synthesis, *Int. J. Chem. Molec. Nucl. Mater. Metal. Eng.*, 2015, vol. 9, p. 1066.
  23. Nozaki, T., Hayashi, K., Miyazaki, Y., and Kajitani, T., Cation distribution dependence on thermoelectric properties of doped spinel M<sub>0.6</sub>Fe<sub>2.4</sub>O<sub>4</sub>, *Mater. Trans.*, 2012, vol. 53, p. 1164.
  24. Shannon, R.D., Revised effective ionic radii and systematic studies of interatomic distances in halides and chalcogenides, *Acta. Crystal.*, 1976, vol. A32, p. 751.
  25. Yaremchenko, A.A., Kovalevsky, A.V., Naumovich, E.N., Kharton, V.V., and Frade, J.R., High-temperature electrical properties of magnesiowustite Mg<sub>1-x</sub>Fe<sub>x</sub>O and spinel Fe<sub>3-x-y</sub>Mg<sub>x</sub>Cr<sub>y</sub>O<sub>4</sub> ceramics, *Solid State Ionics*, 2011, vol. 192, p. 252.
  26. Klemensø, T., Chung, C., Larsen, P.H., and Mogensen, M., The mechanism behind redox instability of anodes in high-temperature SOFCs, *J. Electrochem. Soc.*, 2005, vol. 152, p. 2186.
  27. Mori, M., Yamamoto, T., Itoh, H., Inaba, H., and Tagawa, H., Thermal expansion of nickel–zirconia anodes in Solid Oxide Fuel Cells during fabrication and operation, *J. Electrochem. Soc.*, 1998, vol. 145, p. 1374.
  28. Schneider, F. and Schmalzried, H., Thermodynamic investigation of the system Ni–Fe–O, *Z. Phys. Chem. Neue Folge*, 1990, vol. 166, p. 1.
  29. Rhamdhani, M.A., Hayes, P.C., and Jak, E., Subsolvus phase equilibria of the Fe–Ni–O System, *Metall. Mater. Trans. B*, 2008, vol. 39B, p. 690.

Translated by L. Smolina